Boosting generalized recovery by combined optogenetic stimulation and training after stroke

Running Headline: Stimulation and training boost motor recovery

Emilia Conti[1,2], Anna Letizia Allegra Mascaro[2,3,8], Alessandro Scaglione[1], Giuseppe de Vito[2,4], Francesco Calugi[3,4], Maria Pasquini[5,6], Tommaso Pizzorusso[3,4], Silvestro Micera[5,6], Francesco Saverio Pavone[1,2,7]

1 Department of Physics and Astronomy, University of Florence, 50100 Florence, Italy

2 European Laboratory for Non-linear Spectroscopy University of Florence, 50100 Florence, Italy

3 Neuroscience Institute, National Research Council, Pisa, Italy

4 Department of Neurofarba, University of Florence, 50100 Florence, Italy

5 The BioRobotics Institute and Department of Excellence in Robotics and AI, Scuola Superiore Sant'Anna, Pisa, Italy

6 Bertarelli Foundation Chair in Translational NeuroEngineering, Center for Neuroprosthetics and Institute of Bioengineering, Ecole Polytechnique Federale de Lausanne (EPFL), Lausanne, Switzerland

7 National Institute of Optics, National Research Council, 50100 Florence, Italy

*Corresponding author: Anna Letizia Allegra Mascaro

Via Nello Carrara 1, 50019 Sesto Fiorentino, Florence, Italy

e-mail: allegra@lens.unifi.it

Abstract

An ischemic event is followed by extensive changes in cortical excitability involving both hemispheres. Plasticity in the injured hemisphere plays a crucial role in post-stroke motor recovery and it is a primary target for rehabilitation therapy. Though stimulation of the ipsilesional motor cortex, especially when paired with motor training, facilitates plasticity and functional restoration, the mechanisms underneath the reshaping of cortical functionality are widely unknown. Here, we designed a protocol of optogenetic stimulation of the peri-infarct region as a neuro-plasticizing treatment coupled with a repetitive motor training. This treatment promoted a generalized recovery in forelimb function and the rescue of the essential features of cortical activation profiles during the execution of the motor training. The present work, by exploiting different approaches, provides a fundamental means to better understand the mechanisms underlying the recovery of motor function.

Keywords

Calcium imaging; photothrombotic stroke; rehabilitation; optogenetic stimulation; motor training.

Introduction

Ischemic injuries within the motor cortex result in functional deficits that may profoundly alter the patients' quality of life. Survivors are often chronically impaired in their movements and left with long-term disability [1]. To regain sensory and motor functions after stroke, surviving neural circuits must reorganize [2-4]. Multiple strategies were developed to enhance neural rewiring and dramatically improve motor outcomes [4] including pharmacological treatment, brain stimulation, and motor training. Among them, cortical neuromodulation techniques, such as transcranial magnetic stimulation (TMS) and transcranial direct current stimulation (tDCS), represent a promising non-

invasive approach to improve cortical remapping. Nevertheless, these treatments can induce diffuse and non-specific activation in mixed neuronal populations [5-7]. With the emergence of optogenetics, targeted neuronal populations can be activated or inhibited achieving high temporal and spatial precision [8-11]. Indeed, optogenetics can allow to selectively modify the excitatory/inhibitory balance of brain circuits affected by a stroke lesion [12, 13].

Previous studies have shown that repeated optogenetic neuronal stimulation of the ipsilesional (IL) hemisphere induces a significant improvement in neurovascular coupling response [14]. Furthermore, it has been demonstrated that chronic optogenetic stimulation of the entire cortical mantle promotes behavioral recovery associated with the formation of new and stable thalamocortical synaptic boutons [15]. Even though large-scale remapping is known to be an important factor in the recovery of lost functionalities [16, 17], how the global activity is redistributed over the IL hemisphere after optogenetic stimulation is still largely unknown. Furthermore, several studies have shown that motor practice with the paretic limb during the first weeks after stroke improves functional recovery and behaviorally relevant neural repair both in animal models [18-20] and in humans [21-25]. Neurorehabilitation protocols based on robotic devices have shown to provide promising clinical results. The use of robotic devices in murine models and human patients gives an unbiased evaluation of recovery of motor performances, providing an accurate description of kinetic and kinematic features during rehabilitation after stroke [26-29]. Importantly, it is increasingly recognized that combining stimulation with physical rehabilitation synergistically creates a pro-plasticizing milieu where spared neurons are more susceptible to experience-dependent modifications [4, 30, 31]. To our knowledge, no investigation has yet described

how the combination of optogenetic stimulation and motor training longitudinally molds cortical functional maps in the chronic phase after stroke.

Recent advancements in optical tools, including *in vivo* fluorescence imaging and optogenetics, demonstrated how these techniques are a useful mean to characterize critical features of plasticity, repair and recovery after stroke [32-36].

Here we performed optogenetic stimulation of peri-infarct excitatory neurons and used large-scale optical imaging to dissect remapping and alteration in motor-evoked neuronal activation in the peri-infarct cortex. We observed that the combination of IL optogenetic stimulation and repetitive motor training promotes faster recovery of forelimb function compared to optogenetic stimulation only. Furthermore, the rapid behavioral recovery is associated with the restoration of the critical features of calcium profiles. Finally, we found massive expression of GAP43, a widely known plasticity marker, in the peri-infarct area and axonal sprouting in the contralesional (CL) hemisphere.

Materials and Methods

Mice

All procedures involving mice were performed in accordance with the regulations of the Italian Ministry of Health authorization n. 871/2018. All the experiments have been reported in compliance with the ARRIVE guidelines.

Mice were housed in clear plastic cages under a 12 h light/dark cycle and were given ad libitum access to water and food. We used a transgenic mouse line, C57BL/6J-Tg(Thy1GCaMP6f)GP5.17Dkim/J, from Jackson Laboratories (Bar Harbor, Maine USA). Mice were identified by earmarks and numbered accordingly. Animals were randomly divided into 5 groups. Each group contained comparable numbers of male and female mice (weighing approximately 25g). The age of mice (ranging from 6 to 8 months old)

was consistent between the groups. Animals were randomly distributed (effect size f=0.7; α = 0.05; Power=0.4) in 5 groups as follows: Sham n=4; Stroke n=4; Optostim n=4; Robot n=3; Optostim+Robot (OR) n= 4. Mice that showed no alteration in behavioral experiments after stroke were excluded from the study (n=1).

Channelrhodopsin 2 (ChR2) injection

All surgical procedures were performed under isoflurane anesthesia (3% induction, 1.5% maintenance, in 1L/min oxygen). Body temperature was maintained at 37°C and mice were monitored using respiratory rate and toe pinch throughout the procedure. The animals were placed into a stereotaxic apparatus (Stoelting, Wheat Lane, Wood Dale, IL 60191). The skin over the skull was cut and the periosteum was removed with a blade. We used a dental drill to create a small craniotomy over somatosensory cortex, which was identified by stereotaxic coordinates. Channel rhodopsin injections were performed during the same surgical session in which the photothrombotic lesions were created. We injected 0.5 µL of AAV9-CaMKII-ChR2-mCherry (2.48*1013 GC/mL) 600 µm deep inside the cortex at (i) -0.75 anteroposterior, +1.75 mediolateral. At the end of the rehabilitative period, 30 days after the injection, ChR2 expression is evenly distributed across the cortex layers and it extends for 600 µm in the rostro-caudal direction. In Stroke, Optostim, Robot and OR mice this surgery was followed by the stroke induction. Robot mice were injected with ChR2 though the animals will not optogenetically stimulated. We applied this precaution not to underestimate a possible effect of LED excitation of ChR2 expressing neurons during calcium imaging. In Sham mice a cover glass and an aluminum head-post were attached to the skull using transparent dental cement (Super Bond, C&S), then the animals were placed in a heated cage (temperature 38°) until they fully recovered. Given the design of the experiment, no blind approach was applied during surgery.

Photothrombotic lesion

The primary motor cortex (M1) was identified (stereotaxic coordinates +1,75 lateral, -0.5 rostral from bregma). Five minutes after intraperitoneal injection of Rose Bengal (0.2 ml, 10 mg/ml solution in Phosphate Buffer Saline (PBS); Sigma Aldrich, St. Louis, Missouri, USA), white light from an LED lamp (CL 6000 LED, Carl Zeiss Microscopy, Oberkochen, Germany) was focused with a 20X objective (EC Plan Neofluar NA 0.5, Carl Zeiss Microscopy, Oberkochen, Germany) and used to illuminate the M1 for 15 min to induce unilateral stroke in the right hemisphere. The CTRL animals are not subjected to photothrombosis. A cover glass and an aluminum head-post were attached to the skull using transparent dental cement (Super Bond, C&S). We waited at least 4-5 days after the surgery for the mice to recover before the first imaging session. After the last imaging session, all animals were perfused first with 20-30 mL of 0.01 M PBS (pH 7.6) and then with 150 mL of Paraformaldehyde 4% (PFA, Aldrich, St. Louis, Missouri, USA).

Robotic rehabilitation

Mice were allowed to become accustomed to the apparatus before the first imaging session so that they became acquainted with the new environment. The animals were trained by means of the M-Platform, which is a robotic system that allows mice to perform a retraction movement of their left forelimb [37]. Briefly, the M-Platform is composed of a linear actuator, a 6-axis load cell, a precision linear slide with an adjustable friction system and a custom-designed handle that is fastened to the left wrist of the mouse. The handle is screwed onto the load cell, which permits a complete transfer of the forces applied by the animal to the sensor during the training session. Each training session was divided into “trials” that were repeated sequentially and consisted of 5 consecutive steps. First, the linear actuator moved the handle forward

and extended the mouse left forelimb by 10 mm (full upper extremity extension). Next, the actuator quickly decoupled from the slide and a tone lasting 0.5 s informed the mouse that it should initiate the task. If the animal was able to overcome the static friction (approximately 0.2 N), it voluntarily pulled the handle back by retracting its forelimb (i.e. forelimb flexion back to the starting position). Upon successful completion of the task, a second tone that lasted 1 sec was emitted and the animal was given access to a liquid reward, i.e. 10 µl of sweetened condensed milk, before starting a new cycle. To detect the movement of the wrist of the animal in the low-light condition of the experiment, an infrared (IR) emitter was placed on the linear slide, and rigidly connected to the load cell and thus to the animal's wrist. Slide displacement was recorded by an IR camera (EXIS WEBCAM #17003, Trust) that was placed perpendicular to the antero-posterior axis of the movement. Position and speed signals were subsequently extracted from the video recordings and synchronized with the force signals recorded by the load cell (sampling frequency = 100 Hz). To adjust the friction of the device, a calibration procedure was performed by connecting the actuator with the slide using a rigid component. This component mimics the effect of the retraction movements performed by the animal, reproducing the applied forces in direction and point of application. The training consisted of 15 cycles of passive extension of the affected forelimb followed by its active retraction triggered by the acoustic cue. All groups performed at least one week (5 sessions) of daily training, starting 26 days after injury for Stroke and Optostim mice, 5 days after stroke for Robot and Optostim+Robot groups and after the surgery for Sham animals. During the last week of optogenetic stimulation of Optostim and Stroke mice and the entire rehabilitative period for OR mice the robotic training is followed by the

optogenetic stimulation. Given the design of the experiment, no blind approach was applied during surgery.

Optogenetic stimulation

Awake head-fixed mice were placed under the wide-field microscope to perform daily session of optogenetic stimulation. A blue 473 nm laser is used to deliver 5 Hz, 10ms light pulses similar to Tennant 2017 [15]. The laser power used, ranging from 0.2 to 0.8 mW, was lower than the one necessary to elicit movements of the affected forelimb. Furthermore, the laser power is adjusted during the rehabilitation period, according to the increment of the transfected area and the progressive lowering of stimulation threshold over the weeks. The system is provided with a random-access scanning head, developed using two orthogonally-mounted acousto-optical deflectors (DTSXY400, AA Opto-Electronic). The acousto-optic deflectors rapidly scan lines with a commutation time ~5 µs between a line and the next. After scanning the desired shape (in this case a cross) in the area of the cortex of ChR2 maximum expression (approximately near the injection site -0.75 anteroposterior, +1.75 mediolateral), the acousto-optic deflectors returned to the initial position and repeated the cycle for the total illumination time. The stimulation protocol consists of 3 successive 30 s stimulation daily separated by 1 min rest intervals. All animals (Stroke, Optostim and Optostim+Robot), except for Sham and Robot groups, were stimulated every day for 4 weeks, 5 days after photothrombosis. Optostim and OR groups are exposed to optogenetic stimulation approximately 5 minutes after the execution of the last pulling during motor rehabilitation. We stimulated Stroke mice not expressing ChR2 to evaluate possible artifacts due to repeated laser stimulation. All the experiments

revealed that repeated stimulation of mouse cortex not expressing ChR2 did not affect post-stroke recovery.

Schallert Cylinder Test

Mice were placed in a Plexiglas cylinder (7,5 cm diameter, 16 cm height) and recorded for five minutes by a webcam placed below the cylinder, after 2 minutes of acclimatization. Videos were analyzed frame by frame and the spontaneous use of both forelimbs was assessed during exploration of the walls, by counting the number of contacts performed by the paws of the animal. For each wall exploration, the last paw that left and the first paw that contacted the wall or the ground were assessed. The experimenter was blind to the experimental group. In order to quantify forelimb-use asymmetry displayed by the animal, an Asymmetry index was computed, according to Lai et al. 2015 [38].

Wide-field fluorescence microscope

The custom-made wide-field imaging setup was equipped with two excitation sources allowing imaging of GCaMP6f fluorescence and light-stimulation of ChR2. For imaging of GCaMP6f fluorescence, a 505 nm LED (M505L3 Thorlabs, New Jersey, United States) light was deflected by a dichroic filter (DC FF 495-DI02 Semrock, Rochester, New York USA) on the objective (2.5x EC Plan Neofluar, NA 0.085, Carl Zeiss Microscopy, Oberkochen, Germany). A 3D motorized platform (M-229 for xy plane, M-126 for z-axis movement; Physik Instrumente, Karlsruhe, Germany) allowed sample displacement. The fluorescence signal was selected by a band-pass filter (525/50 Semrock, Rochester, New York USA). Then a 20X objective (LD Plan Neofluar, 20x/0.4 M27, Carl Zeiss Microscopy, Oberkochen, Germany) was used to demagnify the image onto a 100X100 pxl^2 area of the sCMOS camera sensor (OrcaFLASH 4.0, Hamamatsu Photonics, NJ, USA). Images (5.2 x 5.2 mm^2, pixel size 52 µm) were acquired at 25 Hz. To perform

optogenetic stimulation of ChR2, a 473 nm continuous wavelength (CW) laser (OBIS 473nm LX 75mW, Coherent, Santa Clara, California, United States) was overlaid on the imaging path using a second dichroic beam splitter (FF484-FdiO1-25x36, Semrock, Rochester, New York USA) and scanned with two orthogonally-mounted acousto-optical deflectors as previously described (DTSXY400, AA Opto-Electronic, Orsay France).

Image analysis

Analysis of the fluorescence image stacks were previously reported in Allegra et al. 2019. We aimed to characterize activation maps and calcium transient critical features, focusing those transients occurring in the time-window of retraction movement. Briefly, image stacks were registered manually and synchronized to the force data. For all stacks the $\Delta F/F_0$ was computed and 3 seconds time windows were extracted (0.4 sec before and 2.6 sec after) around force peaks that resulted in the movement of the slide. A summed intensity projection (SIP) was then obtained by summing all the time windows in a day of training, this SIP was then thresholded to its median plus one standard deviation to generate a binary image per day. Binary images for each day of a week of training were then superimposed and the common area that was activated in at least 3 days was selected as the region of interest used to extract calcium signal parameters for subsequent analyses. This region of interest was then used to extract the peak amplitude and slope of the $\Delta F/F_0$ for each week of training for each animal (for a formal definition of these measures see Allegra et al. 2019). The experimenter was blind to the experimental group.

Force analysis

To quantify the behavior of each animal on the platform we analyzed the force exerted by the mouse during the retraction phase. For each peak associated with the slide

movement we extracted 4 parameters: 1) peak amplitude as its max value; 2) peak width (full width at half maximum) as the width of the peak at half the peak amplitude; 3) peak area as area of the force signal during its peak width and 4) the time to target as the time between the start of the trial and the peak associated with the last movement of the slide in the trial. The experimenter was blind to the experimental group.

Immunohistochemical analysis

For immunohistochemical analysis of plasticity markers, animals were transcardially perfused with 4% paraformaldehyde. The experimenter was blind to the experimental group. Brains were cut using a vibrating-blade microtome (Leica, Germany) to obtain 100 µm thick coronal sections that were used for immunostaining of NeuN (1:200, Millipore, Germany), Parvalbumin (1:500, Abcam, United Kingdom) and GAP 43 (1:600, Abcam, United Kingdom). The number of Parvalbumin- and GAP43- positive neurons was analyzed using a confocal fluorescence microscope (Nikon Eclipse TE 300, Tokyo, Japan) with a Nikon Plan EPO 60× objective (NA 1.4, oil immersion Nikon, Tokyo, Japan), acquiring 212 µm wide images in the periinfarct cortex. Three sections per animal were analyzed. To evaluate the extension of the lesion we use a 10× objective (C-Apochromat, 0.45 NA, Carl Zeiss Microscopy, Oberkochen, Germany field of view 1.3 mm). Then, the stroke volume for each animal was calculated by summing up all damaged areas and multiplying the number by section thickness and by 3 (the spacing factor). A total volume in mm^3 is given as the mean ± standard deviation of all analyzed animals (n=15).

miRNA quantification

MiR-29a expression was quantified in the cortical ischemic penumbra from the coronal sections previously fixed with PFA. RNA was extracted using Agencourt FormaPure

RNA kit (Beckman Coulter, cat. no. C19157) avoiding the deparaffinization step. The RNA concentration was determined by Nanodrop Spectrophotometer (Thermoscientific 2000 C). MiRNAs were reverse transcribed using TaqMan MicroRNA reverse transcription kit (Applied Biosystems, cat. no. 4366596) and miR-29a gene expression was analyzed by real-time PCR (Step one, Applied Biosystems) using TaqMan inventoried assays for miR29a-3p (assay ID: 002112) and sno234 (assay ID:001234). Quantitative values for cDNA amplification were calculated from the threshold cycle number (Ct) obtained during the exponential growth of the PCR products. The threshold was set automatically by Step one software. Data were analyzed by the ΔΔCt methods using sno234 to normalize the cDNA levels of miR-29a.

Statistical analysis

Statistical analysis was performed using OriginPro software (OriginLab Corporation), setting the significance level at $p<0.05$. The behavioral analysis (Schallert Cylinder test) was performed using two-way ANOVA repeated measure, followed by Tukey and Bonferroni test. For calcium analysis one-way ANOVA was used, followed by Tukey test. For immunohistochemical analysis one-way ANOVA was used, followed by Bonferroni test. For miRNA analysis we used Student's t-test.

Data availability

The data that support the findings of this study are available upon request.

Results

Optogenetic rehabilitation of peri-infarct area restores forelimb functionality but not cortical activation profiles

A focal ischemic lesion was induced in the primary motor cortex (M1) of the right hemisphere on Thy1-GCaMP6f mice (Figure S1A). Peri-infarct excitatory neurons expressing Channelrhodopsin 2 (ChR2), evenly distributed across the cortical layers

(Figure S1B), were the target of our stimulation protocol (Figure 1A). The stimulation paradigm lasted 4 weeks starting 5 days after stroke and consisted of three successive 30-sec laser stimulations trains, separated by 1-min rest intervals (Figure 1B, upper panel). We divided our sample in 3 groups (Figure 1B, lower panel): Sham (no stroke), Stroke (stroke, no ChR2, stimulation), Optostim (stroke, ChR2, stimulation). During the last week of our investigation, right before the optogenetic stimulation protocol, all groups performed motor assessment on a robotic system for mice physical training, the M-Platform [26]. This session allowed us to measure the forces applied and the associated motor-evoked cortical activity. To this aim we exploited a custom-made wide-field microscope [39, 40] characterized by a double illumination path to sequentially perform calcium imaging during the motor assessment and optogenetic stimulation. We longitudinally tested mice forelimb function with Schallert test by quantifying the Asymmetry index (A.i.). While spontaneously recovered mice (Stroke) did not reach pre-stroke levels of A.i., a full recovery of forelimb function was achieved after 4 weeks of optogenetic rehabilitation (Optostim, Figure 1C). We then assessed if behavioral recovery was associated with alteration in motor-evoked cortical functionality by performing wide-field calcium imaging on the affected hemisphere of GCaMP6f mice (Figure 1D, S1C-D). We first analyzed the spatial extension of motor representation by overlapping the movement-triggered activation maps obtained for each day of training. By comparing the activation maps in the 3 experimental groups we observed a segregated activation in healthy mice, whereas in Stroke and Optostim mice the maps covered most of the affected hemisphere (Figure 1E-F). By analyzing the fluorescence signal in the region of maximum activation, we observed that calcium activation of Optostim mice did not recover the features of healthy animals in terms of amplitude and timing (Figure 1G). These combined results demonstrate that, even

though recovery of forelimb function can be achieved by optogenetic stimulation alone, the corresponding motor-evoked calcium activation was dissimilar in spatiotemporal terms to the healthy mice.

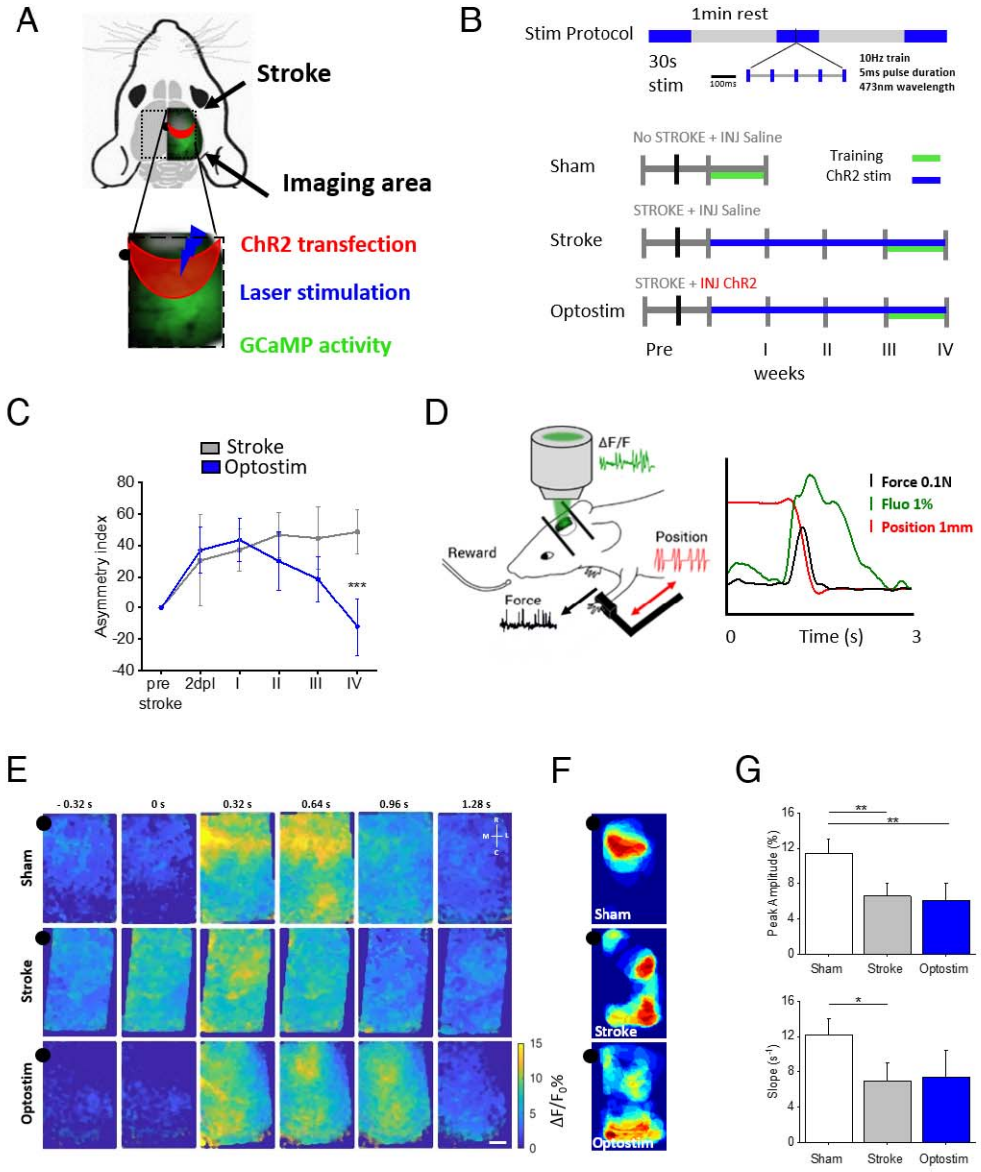
A
Stroke
Imaging area
ChR2 transfection
Laser stimulation
GCaMP activity
B
Stim Protocol
1min rest
30s stim
100ms
10Hz train
5ms pulse duration
473nm wavelength
Sham
No STROKE + INJ Saline
Training
ChR2 stim
Stroke
STROKE + INJ Saline
Optostim
STROKE + INJ ChR2
Pre
I
II
III
IV
weeks
C
Stroke
Optostim
Asymmetry index
80
60
40
20
0
-20
-40
***
pre stroke
2dpl
I
II
III
IV
D
ΔF/F
Reward
Position
Force
Force 0.1N
Fluo 1%
Position 1mm
0
Time (s)
3
E
- 0.32 s
0 s
0.32 s
0.64 s
0.96 s
1.28 s
Sham
Stroke
Optostim
15
10
5
0
ΔF/F0%
F
Sham
Stroke
Optostim
G
Peak Amplitude (%)
16
12
8
4
0
**
**
Sham
Stroke
Optostim
Slope (s-1)
16
12
8
4
0
*
Sham
Stroke
Optostim

Figure 1. Optogenetic stimulation of peri-infarct area: (A) Field of view graphical representation: ChR2-expressing neurons (red area) are stimulated by blue laser. Cortical activity is revealed in the right hemisphere during motor assessment. Grey cloud represents stroke core, black dot represents bregma. (B) Top: stimulation paradigm consisting of 3 stimulation train separated by 1-min rest intervals. Bottom: Sham, Stroke and Optostim experimental timeline. (C) Asymmetry index analysis of Optostim group (blue) compared to non-rehabilitated animals (Stroke group, grey); Optostim vs Stroke two-way ANOVA repeated measure followed by Bonferroni's test: $p<0,0001$. (D) Graphical representation of M-Platform for motor assessment. Graph on the right shows an overlap of simultaneously recorded traces (Force, Fluorescence and Position) of an exemplary retraction movement. (E) Image sequence of cortical activation assessed by calcium imaging during pulling of contralateral forelimb, from 0.32 s before to 1.28 s after the onset of the force peak. Each row shows a representative sequence from a single animal for each group. Black dot represents bregma. Scale bar 1mm. (F) Panels show the average thresholded region of maximum activation triggered by the pulling task for each experimental group. Black dot represents bregma. Scale bar 1mm. (G) Upper panel: graph shows the maximum of fluorescence peaks (average ± SD) of calcium transient (Peak Amplitude_Sham = 11.4 ± 1.6%; Peak Amplitude_Stroke = 6.6 ± 1.5%; Peak Amplitude_Optostim = 6.1 ± 1.9%; one-way ANOVA followed by Tukey's test: pSham-Stroke= 0.007; pSham-Optostim =0.003). Lower panel: graph shows the slope (average ± SD) of the rising phase of fluorescence traces (Slope_Sham = 12.1 ± 1.9 s^{-1}; Slope_Stroke = 6.9 ± 2.0 s^{-1}, Slope_Optostim = 7.4 ± 3.0 s^{-1}; one-way ANOVA followed by Tukey's test: pSham-Stroke = 0.04). nSham=3; nStroke=4; nOptostim=4.

A novel rehabilitation paradigm combining optogenetic stimulation with motor training promotes a generalized recovery

We then wondered if a more effective recovery could be achieved by coupling the same optogenetic stimulation protocol to repetitive motor training of the CL forelimb. We therefore examined the effects of combined optogenetic stimulation and motor training (OR group) and compared it to motor exercise alone (Robot group). The training on the M-Platform started during the acute phase (5 days after stroke) and lasted 4 weeks. In addition to the same physical exercise, right after the motor training, OR mice were exposed to daily optogenetic stimulation of the perilesional cortex along 4 weeks (Figure 2A). By analyzing the force traces associated with the active pulling of the CL forelimb, we observed a progressive modulation of the force peaks in amplitude (Peak Amplitude), width (Full-Width Half Maximum, FWHM) and pulling duration during motor training in OR animals (Figure S1D). Indeed, a reduction trend in the force peak width was observed at the end of the rehabilitative period in OR mice. This was likely attributable to the training on the platform itself since the motor rehabilitation alone (Robot group) induced a similar trend in the force peaks. In addition, the progressive reduction of time-to-target visible in double-treated mice was in line with previous findings in robot-treated stroke mice [26]. We then evaluated through behavioral analysis (Schallert test) alterations in spontaneous forelimbs use. In accordance with Spalletti and colleagues [41], motor training alone was not enough to restore pre-stroke performances (Figure 2B). Conversely, OR mice recovered forelimb function as early as the second week of rehabilitation (Figure 2B).

Considering the faster functional improvement induced by combined rehabilitation compared to optogenetic stimulation alone, we wondered if the behavior mirrored different patterns of motor-evoked cortical activity. To this aim, we assessed the

cortical activation in the affected hemisphere while the awake animals performed the motor training. After 4 weeks of motor rehabilitation, wide-field calcium imaging showed that calcium activation maps of both Robot and OR groups was comparable to healthy controls (Sham) in terms of extension, meaning that daily motor training promotes the refocusing of the cortical motor output 4 weeks after stroke (Figure 2C-D). More in detail, the cortical maps obtained for Robot mice appeared to be shifted towards sensory areas with respect to Sham mice. Furthermore, OR mice activation maps appeared to be more medial with respect to those of healthy mice, suggesting that during the last week of rehabilitation the secondary motor cortex was the principal region of the cortex activated during contralateral forelimb pulling. To verify if these features in motor representation maps were associated with different calcium activity propagation patterns, we analyzed the temporal profile of calcium transients in the region of movement-triggered maximal activation. After classifying the calcium peaks based on the kinematic and dynamic data measured by the M-Platform, we reconstructed the calcium dynamic during force application by the injured forelimb. By comparing the peak amplitude and slope of healthy animals (Sham), non-rehabilitated mice (Stroke), Robot and OR groups, we observed that the treatment with M-Platform alone was not sufficient to induce a full recovery to pre-stroke levels. Conversely, the synergic effect of combined rehabilitation promoted the reestablishment of these salient features of calcium transient in the peri-infarct area (Figure 2E-F). Longitudinal calcium imaging showed a positive trend for OR mice compared to Robot group starting from the second week of rehabilitation (Figure S1E). The pronounced increment in peak amplitude and slope of calcium transient in combined rehabilitated mice became comparable to values distinctive of health condition after 4 weeks of combined treatment.

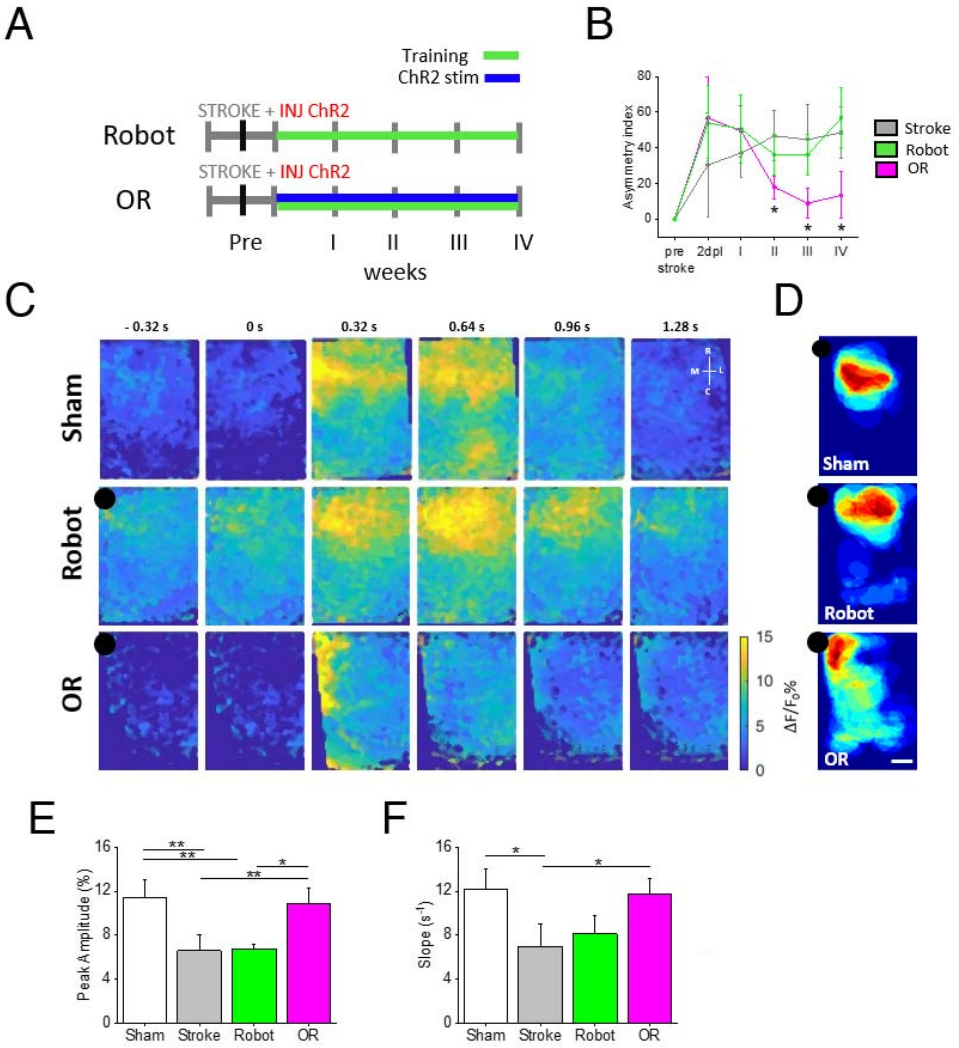

Figure 2. **A novel rehabilitation paradigm combines optogenetic stimulation with motor training:** (A) Experimental timeline for Robot and OR groups. (B) Asymmetry index analysis of Robot (green) and OR (magenta) mice compared to non-rehabilitated animals (Stroke group, grey); OR vs Stroke two-way ANOVA repeated measure of

followed by Bonferroni's test: p-wII=0,005; p-wIII=0,0004; p-wIV=0,0006. nStroke=4; nOR=4. (C) Image sequence of cortical activation during pulling of the handle, from 0.32s before to 1.28s after force peak onset. Each row shows a representative sequence from a single animal of each group Sham (repeated from Figure 1), Robot and OR. Black dot represents bregma. Scale bar 1mm. (D) Panels show the average thresholded ROI computed for each experimental group. Black dot represents bregma. Scale bar 1mm. (E) Graph shows the maximum of fluorescence peaks (average ± SD) of calcium transient (Peak Amplitude_Sham = 11.4 ± 1.6%; Peak Amplitude_Stroke = 6.6 ± 1.5%; Peak Amplitude_Robot = 6.7 ± 0.5%; Peak Amplitude_OR = 10.9 ± 1.4%; one-way ANOVA followed by Tukey's test: pSham-Robot = 0.01; pStroke-OR = 0.009; pRobot-OR=0.02). (F) Graph shows the slope (average ± SD) of the rising phase of fluorescence traces (Slope_Sham = 12.1 ± 1.9 s^{-1}; Slope_Stroke = 6.9 ± 2.0 s^{-1}, Slope_Robot = 8.1 ± 1.6 s^{-1}; Slope_OR = 11.8 ± 1.4 s^{-1}; one-way ANOVA followed by Tukey's test: pStroke-OR = 0.04); nSham=3; nStroke=4; nRobot=3; nOR=4.

Generalized recovery induced by combined rehabilitation is supported by plasticizing and neuroprotective factors

To identify potential mechanisms underlying recovery, we carried out an immunohistochemical analysis to investigate the main actors potentially involved in the recovery. First, we examined the expression of the growth-associated protein 43 (GAP43), a plasticity marker involved in synaptic turnover and reorganization after stroke [2, 42, 43]. While with optogenetic stimulation or motor training GAP43 expression levels were comparable to spontaneously recovered mice, combined rehabilitative treatment promoted a massive expression of this neuronal plasticity marker (Figure 3A, Figure S2A). By analyzing the homotopic areas in the CL hemisphere, we revealed

in Optostim, Robot, and OR mice an increase in number and length of axonal projections (Figure 3B, Figure S2A, right panel) compared to Stroke mice where GAP43 positive fibers (GAP43+) were very infrequent. This suggested that both perilesional stimulation and motor training enhanced the axonal sprouting in distal regions functionally related to the stroke core. Moreover, the combinatorial treatment further boosted the plasticity towards the CL hemisphere.

To test if reshaping of cortical plasticity induced by rehabilitation treatments possibly promoted the recovery of the excitatory/inhibitory balance (Cheng et al., 2014b), profoundly altered by stroke (Jones and Atkins 2015), we evaluated the density of parvalbumin-positive cells (PV+). We observed in the peri-infarct region a significative increase of PV expression in OR mice compared to non-treated animals (Figure 3C). Single treatments were not able to induce a similar level of PV expression (Figure S2B). Together with the increased motor-evoked activation levels in pyramidal cells, the synergic effect of combined rehabilitation could promote the establishment of a new excitatory/inhibitory equilibrium in the peri-infarct and CL hemispheres. Finally, we wondered if a neuroprotective intervention is involved in the restoration of this new balance within the lesioned hemisphere. Since recent work suggested that extracellular glutamate levels reached after stroke can also be regulated by an astrocytic molecular network controlled by miR-29 [44], we analyzed the effects of the combined rehabilitation on the expression levels of miR-29 in the peri-infarct cortex 4 weeks after the lesion. We observed an induction trend of miR-29 expression in OR mice compared to spontaneously recovered mice (Figure S2C). Taken together, the histological analyses show that behavioral and functional improvements after combined rehabilitation are supported by an increased expression of both plasticizing and neuroprotective factors.

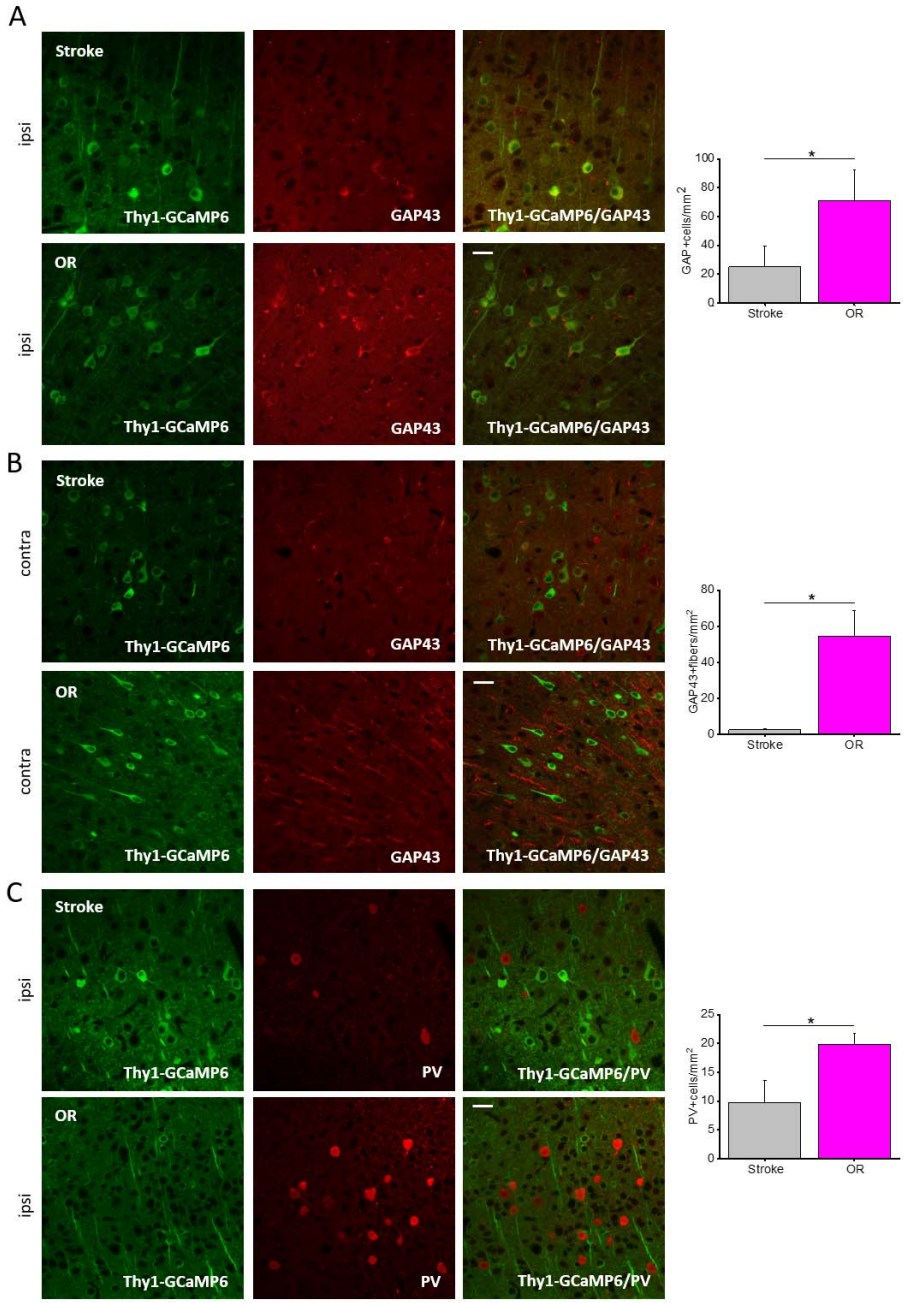
A
Stroke
ipsi
Thy1-GCaMP6
GAP43
Thy1-GCaMP6/GAP43
OR
ipsi
Thy1-GCaMP6
GAP43
Thy1-GCaMP6/GAP43
GAP+cells/mm2
100
80
60
40
20
0
*
Stroke
OR
B
Stroke
contra
Thy1-GCaMP6
GAP43
Thy1-GCaMP6/GAP43
OR
contra
Thy1-GCaMP6
GAP43
Thy1-GCaMP6/GAP43
GAP43+fibers/mm2
80
60
40
20
0
*
Stroke
OR
C
Stroke
ipsi
Thy1-GCaMP6
PV
Thy1-GCaMP6/PV
OR
ipsi
Thy1-GCaMP6
PV
Thy1-GCaMP6/PV
PV+cells/mm2
25
20
15
10
5
0
*
Stroke
OR

Figure 3. *Ex vivo* evaluation highlights the intervention of plasticizing and neuroprotective factors: (A) Left: Transgenic expression of GCaMP6f under Thy1 promoter (green) and representative GAP43 immunostaining (red) of a coronal section (100µm thick) of a Stroke and OR mouse. Right: quantification of GAP43+ cells in the peri-infarct area in Stroke and OR groups (Stroke= 25.0 ± 14.4; OR= 70.7 ± 21.5; one-way ANOVA followed by Bonferroni's test: pStroke-OR= 0,011). (B) Left: transgenic expression of GCaMP6f under Thy1 promoter (green) and representative GAP43 immunostaining (red) of CL labeled fibers. Right: quantification of GAP43+ fibers in the CL hemisphere in Stroke and OR mouse (Stroke= 2.4 ± 0.7; OR= 54.4 ± 14.3; one-way ANOVA followed by Bonferroni's test: pStroke-OR= 0.006); nStroke=4; nOptostim=4; nRobot=3; nOR=4. (C) Left: transgenic expression of GCaMP6f under Thy1 promoter (green) and representative PV immunostaining (red) of a Stroke and OR mouse. Right: quantification of PV+ cells in Stroke and OR groups in the peri-infarct area (Stroke= 9.8 ± 3.8; OR= 19.9 ± 1.9; one-way ANOVA followed by Fisher's test: pStroke-OR= 0.04). Scale bar 20µm.

Discussion

In the present study, we assessed the cortical alterations induced by IL optogenetic stimulation alone and in combination with motor rehabilitation in a mouse model of stroke in the M1. We first evaluated the effect of 4 weeks of repeated IL stimulation. In agreement with a previous work by Tennant and coll. [15], showing that optogenetic stimulation of thalamocortical axons over the entire dorsal cortex enhances the recovery of forepaw sensorimotor abilities, we found that 4 weeks of optogenetic stimulation targeted to ChR2-transfected perilesional cortex lead to a remarkable motor improvement. Nevertheless, our observations indicate that this treatment *per*

se does not recover pre-stroke features of motor-evoked cortical activation. Indeed, a less segregated activation involving almost the entire lesioned hemisphere is observed. The dissociation between behavioral and mesoscale cortical functionality was previously described by Balbi and colleagues in a recent work [45], where post-stroke behavioral impairment was not associated to alterations in functional connectivity. In our study, a possible explanation for behavioral/cortical activity dissociation might lay in the intervention of the CL hemisphere. In detail, during the acute phase after stroke, increases in CL M1 excitability may result in an excessive inhibitory effect on the IL cortex, which may interfere with its reorganization [12, 46-48]. Under the hypothesis that optogenetic stimulation of peri-infarct excitatory neurons counteracts this inhibitory drive by hyper-activating the spared neurons, the recovery of forelimb function might be supported by a new excitatory/inhibitory balance between the two hemispheres. This is in agreement with our previous work [27, 41] showing that the transient inactivation of the homotopic motor cortex was necessary to achieve a generalized recovery. The present study confirms this hypothesis, since stimulating the perilesional neurons might counterbalance the CL inhibitory inference, and eventually lead to an adaptive recovery of forelimb function. Conversely, Robot mice improved their performance on M-Platform during the 4 weeks of treatment but did not achieve a generalized recovery. Nevertheless, repetitive motor training results in higher spatial segregation of the motor-evoked cortical maps of activation. This result suggests that motor training alone promotes task-specific remodeling of cortical connectivity.

Finally, the combined rehabilitative treatment triggers a synergic effect that embraces both behavioral and functional spheres. Indeed, asymmetry index analysis indicated that the combination of these two strategies induces a faster restoration of the forelimb function towards healthy conditions, as measured via Schallert test. Indeed,

forelimb function was already restored to pre-stroke levels at the end of the second week of combined rehabilitation, 2 weeks before the optostimulation-treated mice. At the same time, flanking the stimulation with repeated exercise promoted both behavioral improvement and progressive segregation of motor-associated circuitry in the peri-lesioned cortex.

The behavioral improvement is supported by the long-lasting expression of growth-associated factors in the perilesional area, as demonstrated by the increased number of cells expressing GAP43, known to promote both cortical remapping [2] and axonal sprouting [2, 42, 43] after stroke. This result is in agreement with Spalletti and collaborators [41] showing that a combined rehabilitative treatment promotes an increase of plasticity marker expression. Accordingly, we see an increase in motor-evoked cortical activation in parallel with a more pronounced segregation mediated by excitatory cells in the peri-infarct area of OR mice compared to single treatments (Optostim and Robot groups) and spontaneous recovery (Stroke group). Together with the higher levels of parvalbumin expression, these results suggest that the combined treatment might promote the restoration of excitatory/inhibitory balance in the peri-infarct cortex.

The recovery of the excitatory/inhibitory balance appears to be further supported by the axonal sprouting in the CL cortex, where a substantial number of GAP43+ fibers were detected, especially in combined rehabilitated mice. The increment of GAP43+ cells in the peri-infarct area, in combination with GAP43+ axons in the CL region, suggests the arise of transcallosal axonal sprouting from the IL hemisphere. In addition, our results show a modest increase in miR-29 expression following optical stimulation in line with previous studies of miR-29 in stroke animal models showing improved outcomes upon augmented miRNA levels [49, 50]. Considering the role of miR-

29 in modulating glutamate levels in the lesioned tissue [44], our findings reinforce the hypothesis on the neuroprotective action of miRNA in the injured brain.

Acknowledgments

We thank K. Deisseroth for opsin plasmids. We thank Matteo Caleo, Cristina Spalletti and Claudia Alia for very useful discussion about the manuscript. This project has received funding from the H2020 EXCELLENT SCIENCE - European Research Council (ERC) under grant agreement 692943 BrainBIT. In addition, it was supported by the European Union's Horizon 2020 Research and Innovation Programme under Grant Agreements 785907 (HBP SGA2), and 654148 (Laserlab-Europe). Part of this work was performed within the framework of the Proof of Concept Studies for the ESFRI research infrastructure project Euro-BioImaging at the PCS facility LENS.

Author Contributions

E.C. and A.L.A.M. conceived the study. E.C. and A.L.A.M. performed experiments. E.C., A.S., G.d.V., M.P., and F.C. processed data. F.S.P., T.P. and S.M. obtained funding support. E.C. and A.L.A.M. wrote the paper. All authors approved the paper.

Declaration of conflicting interests

The authors declare no competing interests.

References

1. Schwab ME. How hard is the CNS hardware? *Nat Neurosci* 2010; 13: 1444-1446. 2010/11/26. DOI: 10.1038/nn1210-1444.
2. Murphy TH and Corbett D. Plasticity during stroke recovery: from synapse to behaviour. *Nat Rev Neurosci* 2009; 10: 861-872. 2009/11/06. DOI: 10.1038/nrn2735.
3. Dancause N and Nudo RJ. Shaping plasticity to enhance recovery after injury. *Prog Brain Res* 2011; 192: 273-295. 2011/07/19. DOI: 10.1016/B978-0-444-53355-5.00015-4.

4. Zeiler SR and Krakauer JW. The interaction between training and plasticity in the poststroke brain. *Curr Opin Neurol* 2013; 26: 609-616. 2013/10/19. DOI: 10.1097/WCO.0000000000000025.
5. Takatsuru Y, Fukumoto D, Yoshitomo M, et al. Neuronal circuit remodeling in the contralateral cortical hemisphere during functional recovery from cerebral infarction. *J Neurosci* 2009; 29: 10081-10086. 2009/08/14. DOI: 10.1523/JNEUROSCI.1638-09.2009.
6. Iwai M, Stetler RA, Xing J, et al. Enhanced oligodendrogenesis and recovery of neurological function by erythropoietin after neonatal hypoxic/ischemic brain injury. *Stroke* 2010; 41: 1032-1037. 2010/04/03. DOI: 10.1161/STROKEAHA.109.570325.
7. Zhao Y and Rempe DA. Targeting astrocytes for stroke therapy. *Neurotherapeutics* 2010; 7: 439-451. 2010/10/01. DOI: 10.1016/j.nurt.2010.07.004.
8. Boyden ES, Zhang F, Bamberg E, et al. Millisecond-timescale, genetically targeted optical control of neural activity. *Nat Neurosci* 2005; 8: 1263-1268. 2005/08/24. DOI: 10.1038/nn1525.
9. Li N, Daie K, Svoboda K, et al. Robust neuronal dynamics in premotor cortex during motor planning. *Nature* 2016; 532: 459-464. 2016/04/14. DOI: 10.1038/nature17643.
10. Yizhar O, Fenno LE, Davidson TJ, et al. Optogenetics in neural systems. *Neuron* 2011; 71: 9-34. 2011/07/13. DOI: 10.1016/j.neuron.2011.06.004.
11. Wahl AS, Buchler U, Brandli A, et al. Optogenetically stimulating intact rat corticospinal tract post-stroke restores motor control through regionalized functional circuit formation. *Nat Commun* 2017; 8: 1187. 2017/11/01. DOI: 10.1038/s41467-017-01090-6.
12. Murase N, Duque J, Mazzocchio R, et al. Influence of interhemispheric interactions on motor function in chronic stroke. *Ann Neurol* 2004; 55: 400-409. 2004/03/03. DOI: 10.1002/ana.10848.
13. Volz LJ, Vollmer M, Michely J, et al. Time-dependent functional role of the contralesional motor cortex after stroke. *Neuroimage Clin* 2017; 16: 165-174. 2017/08/11. DOI: 10.1016/j.nicl.2017.07.024.
14. Cheng MY, Wang EH, Woodson WJ, et al. Optogenetic neuronal stimulation promotes functional recovery after stroke. *Proc Natl Acad Sci U S A* 2014; 111: 12913-12918. 2014/08/20. DOI: 10.1073/pnas.1404109111.
15. Tennant KA, Taylor SL, White ER, et al. Optogenetic rewiring of thalamocortical circuits to restore function in the stroke injured brain. *Nat Commun* 2017; 8: 15879. 2017/06/24. DOI: 10.1038/ncomms15879.
16. Siegel JS, Ramsey LE, Snyder AZ, et al. Disruptions of network connectivity predict impairment in multiple behavioral domains after stroke. *Proc Natl Acad Sci U S A* 2016; 113: E4367-4376. 2016/07/13. DOI: 10.1073/pnas.1521083113.
17. Siegel JS, Seitzman BA, Ramsey LE, et al. Re-emergence of modular brain networks in stroke recovery. *Cortex* 2018; 101: 44-59. 2018/02/08. DOI: 10.1016/j.cortex.2017.12.019.
18. Nudo RJ, Wise BM, SiFuentes F, et al. Neural substrates for the effects of rehabilitative training on motor recovery after ischemic infarct. *Science* 1996; 272: 1791-1794. 1996/06/21.

19. Biernaskie J and Corbett D. Enriched rehabilitative training promotes improved forelimb motor function and enhanced dendritic growth after focal ischemic injury. *J Neurosci* 2001; 21: 5272-5280. 2001/07/05.
20. Jones TA, Chu CJ, Grande LA, et al. Motor skills training enhances lesion-induced structural plasticity in the motor cortex of adult rats. *J Neurosci* 1999; 19: 10153-10163. 1999/11/13.
21. Jaillard A, Martin CD, Garambois K, et al. Vicarious function within the human primary motor cortex? A longitudinal fMRI stroke study. *Brain* 2005; 128: 1122-1138. 2005/02/25. DOI: 10.1093/brain/awh456.
22. Butefisch CM. Neurobiological bases of rehabilitation. *Neurol Sci* 2006; 27 Suppl 1: S18-23. 2006/05/19. DOI: 10.1007/s10072-006-0540-z.
23. Dong Y, Winstein CJ, Albistegui-DuBois R, et al. Evolution of FMRI activation in the perilesional primary motor cortex and cerebellum with rehabilitation training-related motor gains after stroke: a pilot study. *Neurorehabil Neural Repair* 2007; 21: 412-428. 2007/03/21. DOI: 10.1177/1545968306298598.
24. Liepert J, Graef S, Uhde I, et al. Training-induced changes of motor cortex representations in stroke patients. *Acta Neurol Scand* 2000; 101: 321-326. 2000/09/15.
25. Sawaki L, Butler AJ, Leng X, et al. Constraint-induced movement therapy results in increased motor map area in subjects 3 to 9 months after stroke. *Neurorehabil Neural Repair* 2008; 22: 505-513. 2008/09/11. DOI: 10.1177/1545968308317531.
26. Spalletti C, Lai S, Mainardi M, et al. A robotic system for quantitative assessment and poststroke training of forelimb retraction in mice. *Neurorehabil Neural Repair* 2014; 28: 188-196. 2013/11/12. DOI: 10.1177/1545968313506520.
27. Allegra Mascaro AL, Conti E, Lai S, et al. Combined Rehabilitation Promotes the Recovery of Structural and Functional Features of Healthy Neuronal Networks after Stroke. *Cell Rep* 2019; 28: 3474-3485 e3476. 2019/09/26. DOI: 10.1016/j.celrep.2019.08.062.
28. Hogan N and Krebs HI. Physically interactive robotic technology for neuromotor rehabilitation. *Prog Brain Res* 2011; 192: 59-68. 2011/07/19. DOI: 10.1016/B978-0-444-53355-5.00004-X.
29. Balasubramanian S, Klein J and Burdet E. Robot-assisted rehabilitation of hand function. *Curr Opin Neurol* 2010; 23: 661-670. 2010/09/21. DOI: 10.1097/WCO.0b013e32833e99a4.
30. Alia C, Spalletti C, Lai S, et al. Neuroplastic Changes Following Brain Ischemia and their Contribution to Stroke Recovery: Novel Approaches in Neurorehabilitation. *Front Cell Neurosci* 2017; 11: 76. 2017/04/01. DOI: 10.3389/fncel.2017.00076.
31. Straudi S, Martinuzzi C, Baroni A, et al. Monitoring Step Activity During Task-Oriented Circuit Training in High-Functioning Chronic Stroke Survivors: A Proof-of-Concept Feasibility Study. *Ann Rehabil Med* 2016; 40: 989-997. 2017/01/26. DOI: 10.5535/arm.2016.40.6.989.
32. Sakadzic S, Lee J, Boas DA, et al. High-resolution in vivo optical imaging of stroke injury and repair. *Brain Res* 2015; 1623: 174-192. 2015/05/12. DOI: 10.1016/j.brainres.2015.04.044.

33. Cheng MY, Wang EH and Steinberg GK. Optogenetic Approaches to Study Stroke Recovery. *ACS Chemical Neuroscience* 2014; 5: 1144-1145. DOI: 10.1021/cn500216f.
34. Pendharkar AV, Levy SL, Ho AL, et al. Optogenetic modulation in stroke recovery. 2016; 40: E6. DOI: 10.3171/2016.2.Focus163.
35. Montagni E, Resta F, Mascaro ALA, et al. Optogenetics in Brain Research: From a Strategy to Investigate Physiological Function to a Therapeutic Tool. *Photonics* 2019; 6: 92.
36. Bauer AQ, Kraft AW, Wright PW, et al. Optical imaging of disrupted functional connectivity following ischemic stroke in mice. *Neuroimage* 2014; 99: 388-401. 2014/05/28. DOI: 10.1016/j.neuroimage.2014.05.051.
37. Pasquini M, Lai S, Spalletti C, et al. A Robotic System for Adaptive Training and Function Assessment of Forelimb Retraction in Mice. *IEEE Trans Neural Syst Rehabil Eng* 2018; 26: 1803-1812. 2018/08/15. DOI: 10.1109/TNSRE.2018.2864279.
38. Lai S, Panarese A, Spalletti C, et al. Quantitative kinematic characterization of reaching impairments in mice after a stroke. *Neurorehabil Neural Repair* 2015; 29: 382-392. 2014/10/18. DOI: 10.1177/1545968314545174.
39. Conti E, Allegra Mascaro AL and Pavone FS. Large Scale Double-Path Illumination System with Split Field of View for the All-Optical Study of Inter-and Intra-Hemispheric Functional Connectivity on Mice. *Methods Protoc* 2019; 2 2019/06/06. DOI: 10.3390/mps2010011.
40. Crocini C, Ferrantini C, Coppini R, et al. Optogenetics design of mechanistically-based stimulation patterns for cardiac defibrillation. *Sci Rep* 2016; 6: 35628. 2016/10/18. DOI: 10.1038/srep35628.
41. Spalletti C, Alia C, Lai S, et al. Combining robotic training and inactivation of the healthy hemisphere restores pre-stroke motor patterns in mice. *Elife* 2017; 6 2017/12/28. DOI: 10.7554/eLife.28662.
42. Carmichael ST. Plasticity of cortical projections after stroke. *Neuroscientist* 2003; 9: 64-75. 2003/02/13. DOI: 10.1177/1073858402239592.
43. Carmichael ST, Archibeque I, Luke L, et al. Growth-associated gene expression after stroke: evidence for a growth-promoting region in peri-infarct cortex. *Exp Neurol* 2005; 193: 291-311. 2005/05/05. DOI: 10.1016/j.expneurol.2005.01.004.
44. Kobayashi M, Benakis C, Anderson C, et al. AGO CLIP Reveals an Activated Network for Acute Regulation of Brain Glutamate Homeostasis in Ischemic Stroke. *Cell Rep* 2019; 28: 979-991 e976. 2019/07/25. DOI: 10.1016/j.celrep.2019.06.075.
45. Balbi M, Vanni MP, Vega MJ, et al. Longitudinal monitoring of mesoscopic cortical activity in a mouse model of microinfarcts reveals dissociations with behavioral and motor function. *J Cereb Blood Flow Metab* 2018: 271678X18763428. 2018/03/10. DOI: 10.1177/0271678X18763428.
46. Buetefisch CM. Role of the Contralesional Hemisphere in Post-Stroke Recovery of Upper Extremity Motor Function. *Front Neurol* 2015; 6: 214. 2015/11/04. DOI: 10.3389/fneur.2015.00214.

47. Butefisch CM, Wessling M, Netz J, et al. Relationship between interhemispheric inhibition and motor cortex excitability in subacute stroke patients. *Neurorehabil Neural Repair* 2008; 22: 4-21. 2007/05/18. DOI: 10.1177/1545968307301769.
48. Shimizu T, Hosaki A, Hino T, et al. Motor cortical disinhibition in the unaffected hemisphere after unilateral cortical stroke. *Brain* 2002; 125: 1896-1907. 2002/07/24. DOI: 10.1093/brain/awf183.
49. Khanna S, Rink C, Ghoorkhanian R, et al. Loss of miR-29b following acute ischemic stroke contributes to neural cell death and infarct size. *J Cereb Blood Flow Metab* 2013; 33: 1197-1206. 2013/05/02. DOI: 10.1038/jcbfm.2013.68.
50. Ouyang M, Su W, Xiao L, et al. Modulation by miR-29b of intestinal epithelium homoeostasis through the repression of menin translation. *Biochem J* 2015; 465: 315-323. 2014/10/16. DOI: 10.1042/BJ20141028.

Supplementary Figures

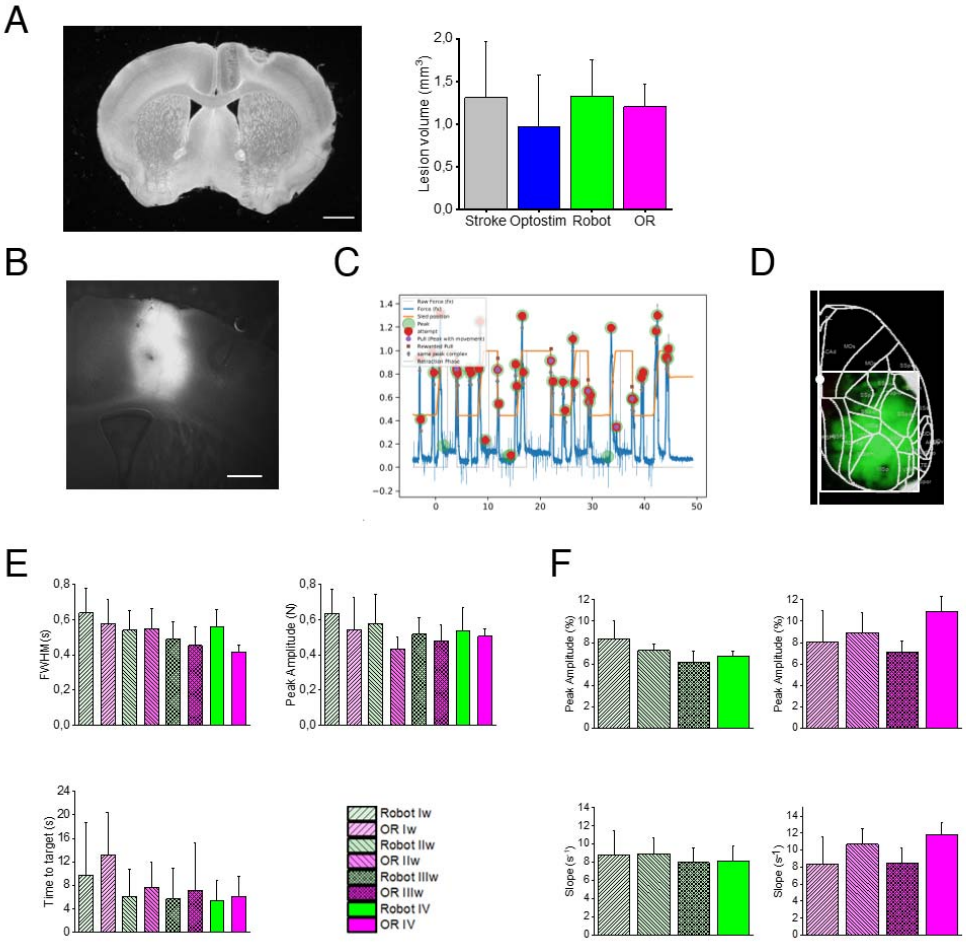

Supplementary Figure 1. (A) Coronal section of a mouse brain 30 days after photothrombosis, 1 mm scale bar. The right panel shows the quantification of the lesioned area in the experimental groups (Stroke= 1.3 ± 0.6; Optostim= 0.9 ± 0.6; Robot= 1.3 ± 0.4; OR= 1.2 ± 0.3). (B) Coronal section of a mouse brain transfected with ChR2 30 days after the injection, 0.5 mm scale bar. (C) Force trace (in blue) registered

by the load cell of M-Platform during a training session. The force analysis showed the sled position during the session (in orange), the attempts to reach the home position (red spot), the force peaks associated to movement (violet spot) and the pulling associated with reward (bordeaux square). (D) Graphical representation of functional regions of the cortex included in the imaging area (white square). The white spot indicates bregma. (E) Force analysis during pulling task (average ± SD). Left upper panel shows the Full Width Half Maximum of the force peak (Robot_Iw= 0.64 ± 0.14; OR_Iw= 0.58 ± 0.14; Robot_IIw= 0.54 ± 0.11; OR_IIw= 0.55 ± 0.11; Robot_IIIw= 0.49 ± 0.10; OR_IIIw= 0.45 ± 0.11; Robot_IVw= 0.56 ± 0.10; OR_IVw= 0.42 ± 0.04). Right upper panel show the Peak Amplitude (Robot_Iw= 0.63 ± 0.14; OR_Iw= 0.54 ± 0.18; Robot_IIw= 0.58 ± 0.17; OR_IIw= 0.43 ± 0.06; Robot_IIIw= 0.52 ± 0.09; OR_IIIw= 0.48 ± 0.09; Robot_IVw= 0.54 ± 0.13; OR_IVw= 0.5 ± 0.04) and the lower panel shows the Time to Target (Robot_Iw= 9.7 ± 8.9; OR_Iw= 13.2 ± 7.2; Robot_IIw= 6.1 ± 4.6; OR_IIw= 7.6 ± 4.3; Robot_IIIw= 5.6 ± 5.2; OR_IIIw= 7.1 ± 8.1; Robot_IVw= 5.4 ± 3.4; OR_IVw= 6.0± 3.6); nRobot=8; nOR=4. (E) Longitudinal analysis of cortical activation profiles over the 4 weeks for Robot (Amplitude: Iw= 8.3 ± 1.7; IIw= 7.3± 0.6; III= 6.1± 1.1; IV= 6.7 ±0.5; Slope: Iw= 8.8± 2.6; IIw= 8.9 ± 1.8; III= 8.0 ± 1.6; IV= 8.1 ± 1.6) and OR groups (Amplitude: Iw=8.1 ± 2.9; IIw= 8.9 ± 1.9; III= 7.1 ± 1.0; IV= 10.9 ± 1.4; Slope: Iw= 8.3 ± 3.3; IIw= 10.7 ± 2.9; III= 8.4 ± 1.8; IV= 11.8 ± 1.4).

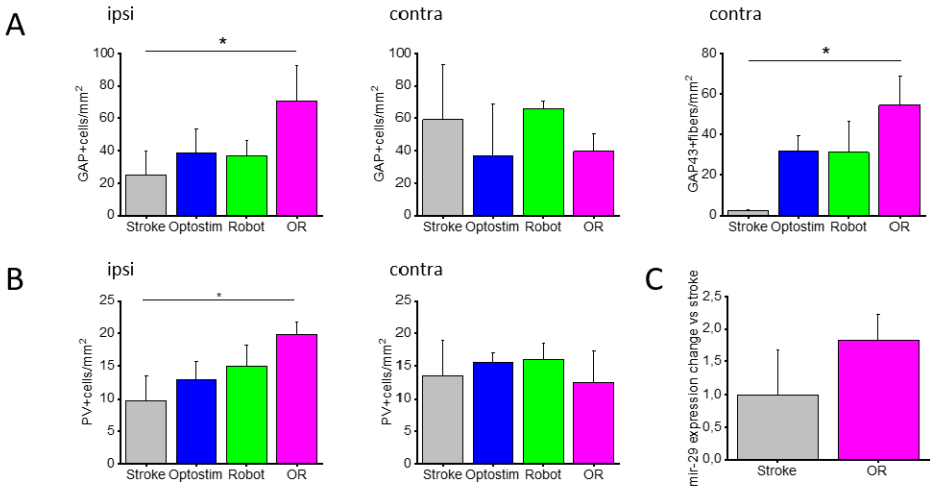

Supplementary Figure 2. (A) Immunohistochemical analysis of the ipsilesional (left panel) and contralesional hemisphere of GAP43+ cells for the experimental groups. Left panel shows the quantification of GAP43+ cells in the experimental groups in the peri-infarct area (Stroke= 25.0 ± 14.4; Optostim= 38.7 ± 14.5; Robot= 36.7 ± 9.7; OR= 70,7 ± 21.5; one-way ANOVA followed by Fisher's test: pStroke-OR= 0.011). Middle panel shows the quantification of GAP43+ cells in the contralesional hemisphere (Stroke= 59.1 ± 33.9; Optostim= 36.5 ± 32.2; Robot= 66.1 ± 4.5; OR=39.6 ± 10.7). Right panel shows the quantification of GAP43+ fibers in the experimental groups in the ipsilesional area (Stroke= 2.4 ± 0.7; Optostim= 31.8 ± 7.7; Robot= 31.2 ± 15.2; OR= 54.4 ± 14.3; one-way ANOVA followed by Bonferroni's test: pStroke-OR= 0.006). (B) Immunohistochemical analysis of the ipsilesional (left panel) and contralesional hemisphere of PV positive cells for the experimental groups. Left panel shows the quantification of PV+ cells in the experimental groups in the peri-infarct area (Stroke=

9.8 ± 3.8; Optostim= 13.0 ± 2.6; Robot= 14.9 ± 3.2; OR= 19.9 ± 1.9; one-way ANOVA followed by Bonferroni's test: pStroke-OR= 0.006). Right panel show the quantification of PV+ cells in the contralesional hemisphere (Stroke= 13.6 ± 5.3; Optostim= 15.5 ± 1.4; Robot= 16.0 ± 2.4; OR= 12.6 ± 4.7). (C) Quantification of the ipsilesional expression of miR29 in Stroke and OR groups (Stroke= 1.0 ± 0.7; OR= 1.8 ± 0.4; pStroke-OR= 0.09).

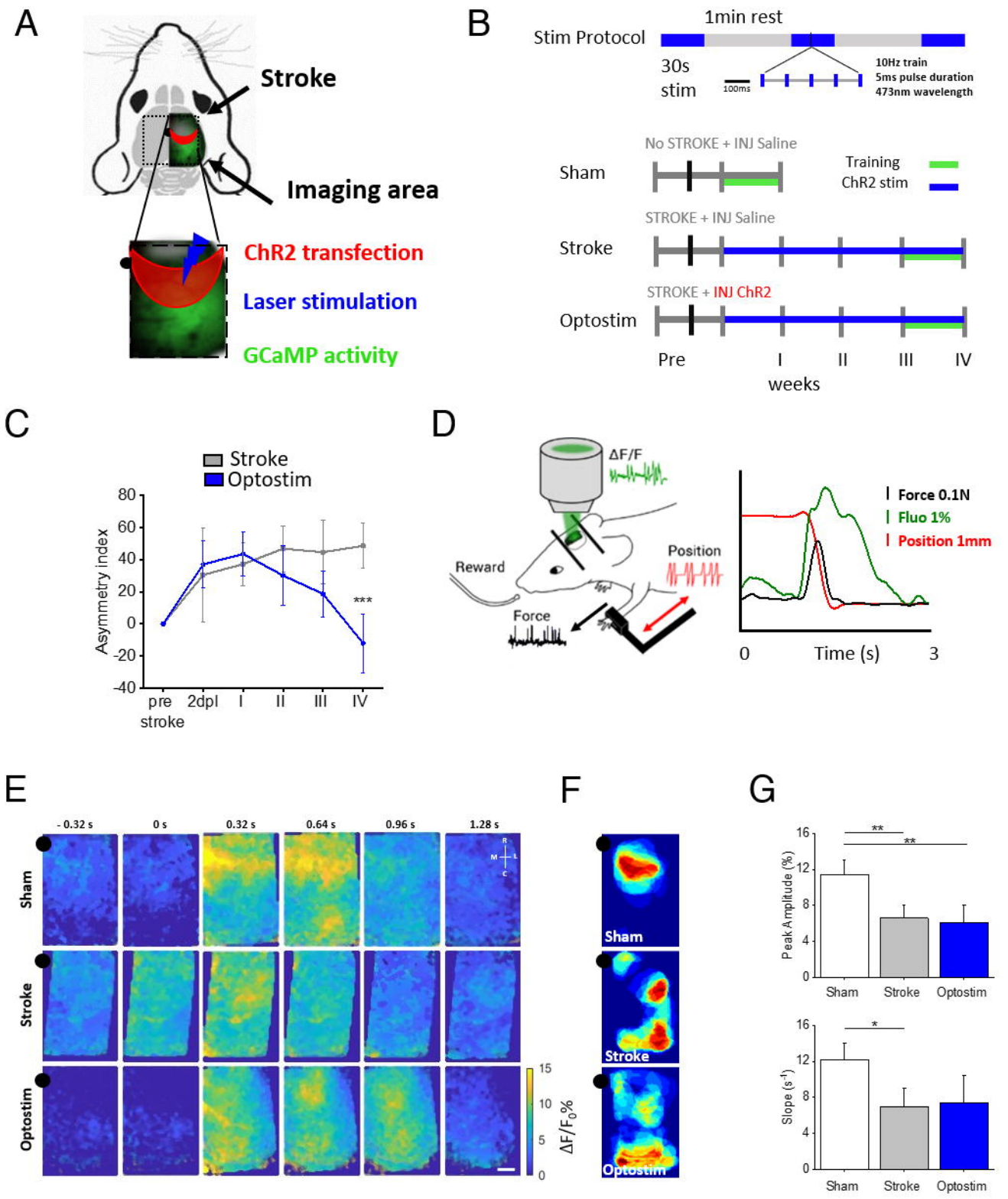
A
Stroke
Imaging area
ChR2 transfection
Laser stimulation
GCaMP activity
B
Stim Protocol
1min rest
30s stim
100ms
10Hz train
5ms pulse duration
473nm wavelength
No STROKE + INJ Saline
Sham
Training
ChR2 stim
STROKE + INJ Saline
Stroke
STROKE + INJ ChR2
Optostim
Pre
I
II
III
IV
weeks
C
Stroke
Optostim
Asymmetry index
80
60
40
20
0
-20
-40
***
pre stroke
2dpI
I
II
III
IV
D
ΔF/F
Reward
Position
Force
Force 0.1N
Fluo 1%
Position 1mm
0
Time (s)
3
E
- 0.32 s
0 s
0.32 s
0.64 s
0.96 s
1.28 s
Sham
Stroke
Optostim
15
10
5
0
ΔF/F0%
F
Sham
Stroke
Optostim
G
Peak Amplitude (%)
16
12
8
4
0
**
**
Sham
Stroke
Optostim
Slope (s-1)
16
12
8
4
0
*
Sham
Stroke
Optostim

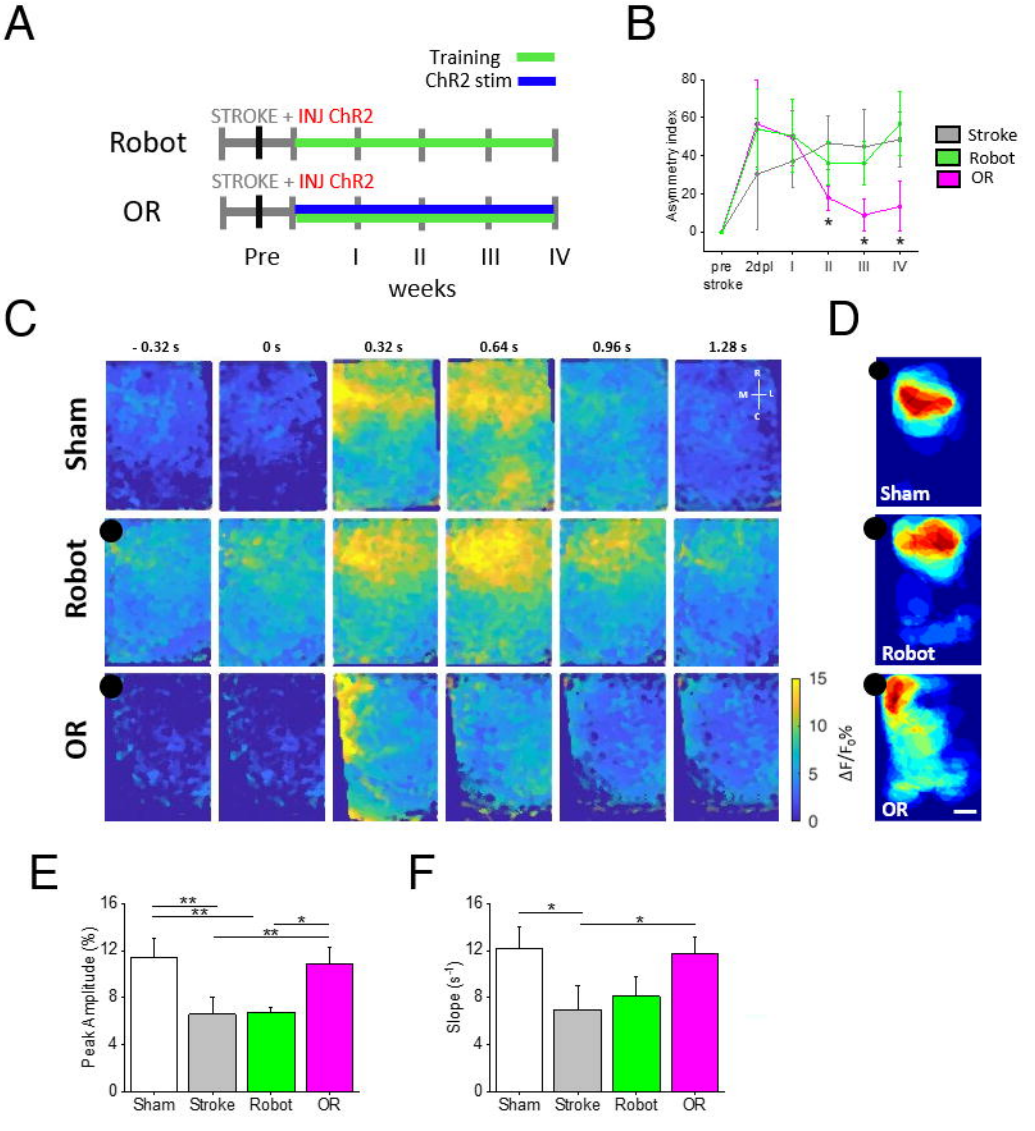
A
Training
ChR2 stim
STROKE + INJ ChR2
Robot
STROKE + INJ ChR2
OR
Pre
I
II
III
IV
weeks
B
Asymmetry index
80
60
40
20
0
pre stroke
2dpl
I
II
III
IV
Stroke
Robot
OR
C
- 0.32 s
0 s
0.32 s
0.64 s
0.96 s
1.28 s
Sham
Robot
OR
15
10
5
0
ΔF/F0%
D
Sham
Robot
OR
E
Peak Amplitude (%)
16
12
8
4
0
Sham
Stroke
Robot
OR
F
Slope (s-1)
16
12
8
4
0
Sham
Stroke
Robot
OR

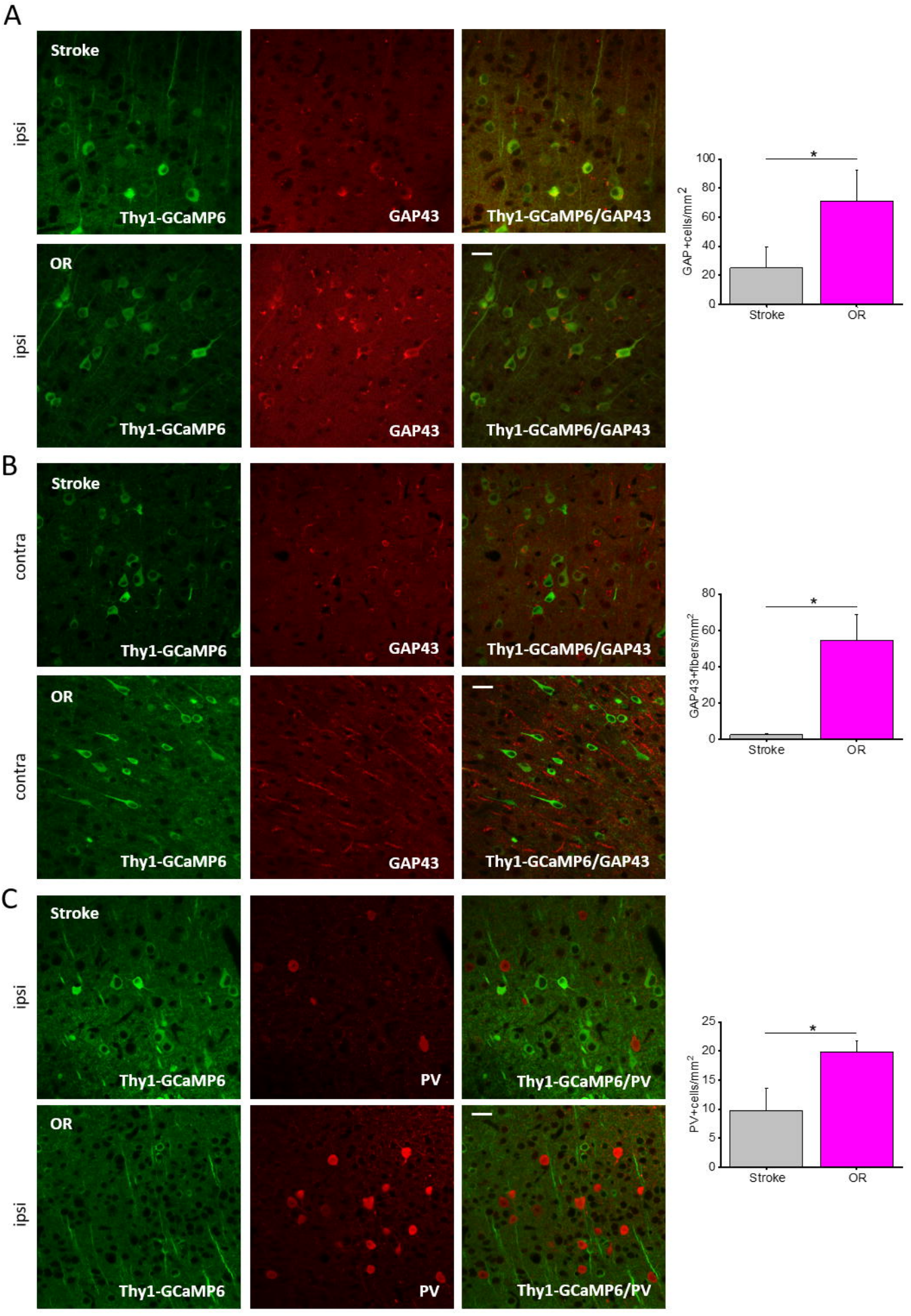
A
Stroke
ipsi
Thy1-GCaMP6
GAP43
Thy1-GCaMP6/GAP43
OR
ipsi
Thy1-GCaMP6
GAP43
Thy1-GCaMP6/GAP43
GAP+cells/mm2
100
80
60
40
20
0
*
Stroke
OR
B
Stroke
contra
Thy1-GCaMP6
GAP43
Thy1-GCaMP6/GAP43
OR
contra
Thy1-GCaMP6
GAP43
Thy1-GCaMP6/GAP43
GAP43+fibers/mm2
80
60
40
20
0
*
Stroke
OR
C
Stroke
ipsi
Thy1-GCaMP6
PV
Thy1-GCaMP6/PV
OR
ipsi
Thy1-GCaMP6
PV
Thy1-GCaMP6/PV
PV+cells/mm2
25
20
15
10
5
0
*
Stroke
OR

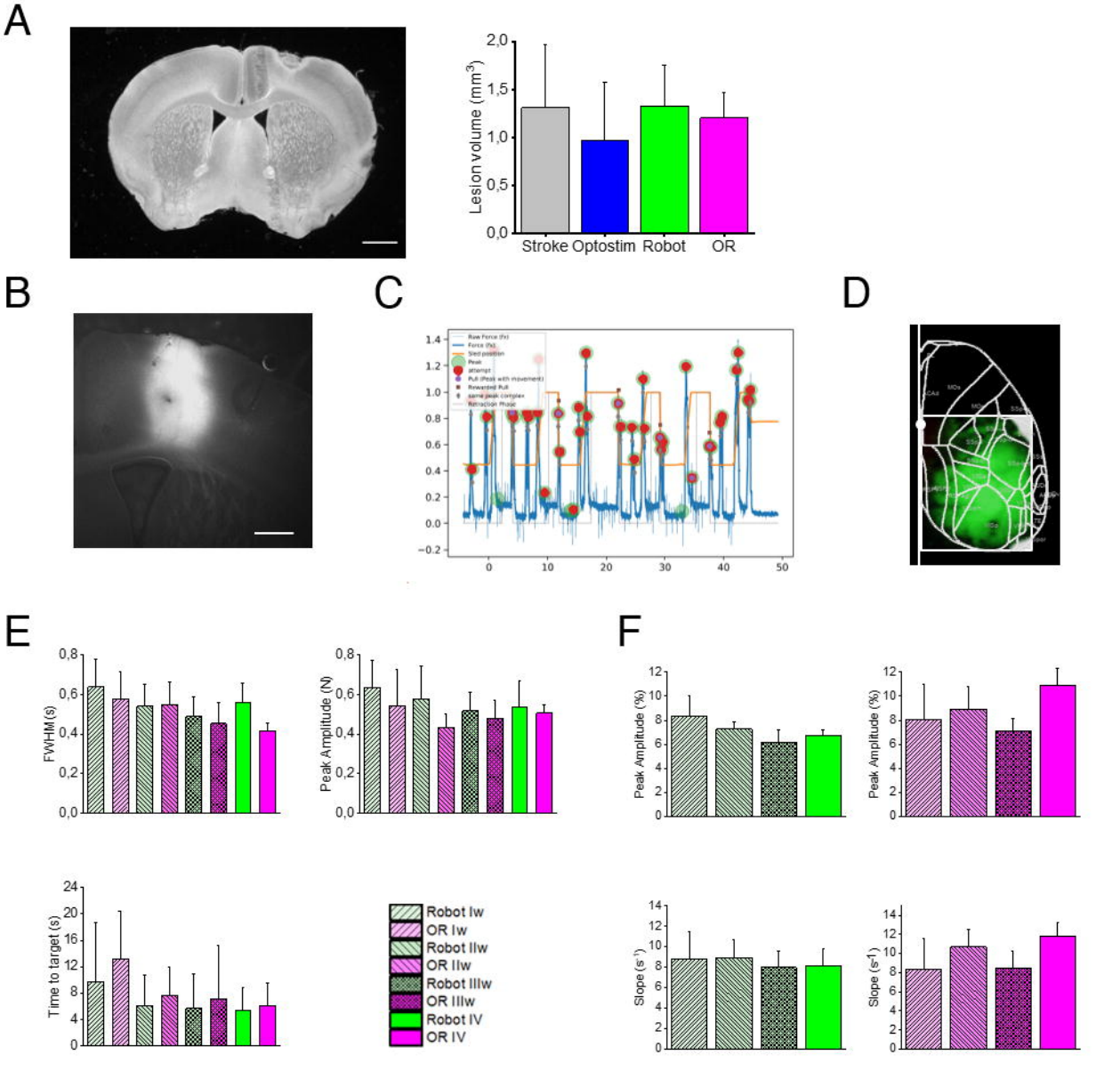
A
Lesion volume (mm3)
2,0
1,5
1,0
0,5
0,0
Stroke
Optostim
Robot
OR
B
C
D
E
FWHM (s)
Peak Amplitude (N)
Time to target (s)
F
Peak Amplitude (%)
Slope (s-1)
Robot Iw
OR Iw
Robot IIw
OR IIw
Robot IIIw
OR IIIw
Robot IV
OR IV

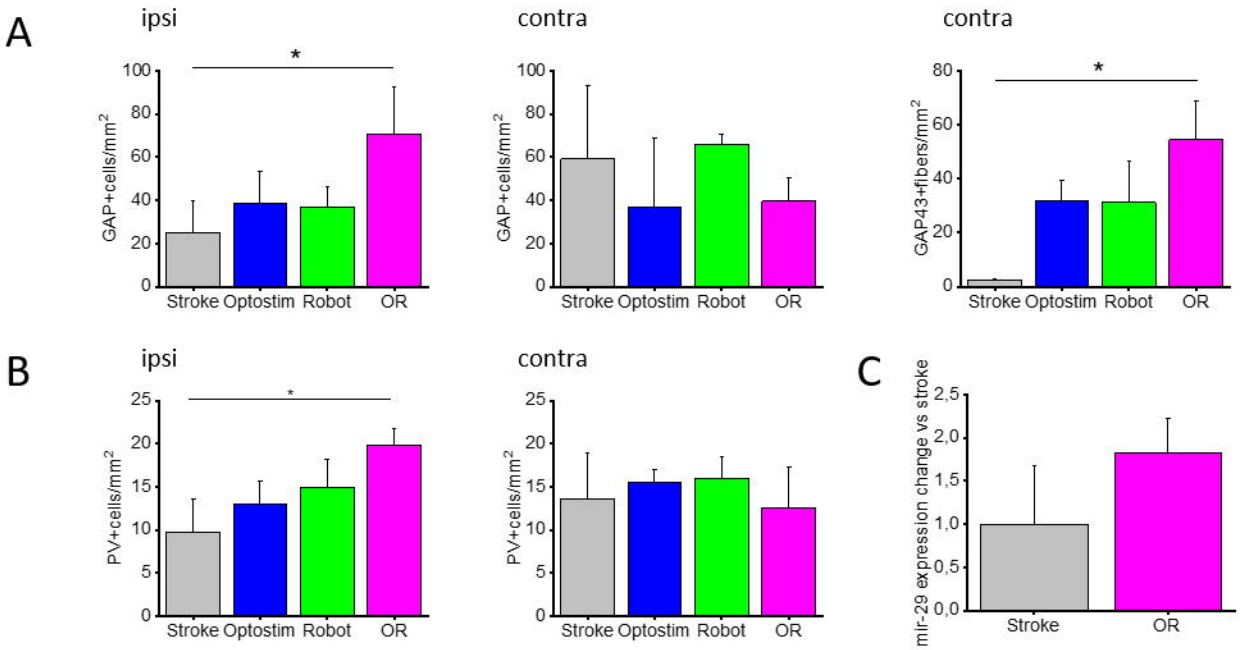
A
ipsi
contra
contra
GAP+cells/mm2
GAP43+fibers/mm2
Stroke
Optostim
Robot
OR
*
B
ipsi
contra
PV+cells/mm2
C
mir-29 expression change vs stroke
Stroke
OR